Proceedings of IMECE'02
2002 ASME International Mechanical Engineering Congress & Exposition
New Orleans, Louisiana, November 17-22, 2002

IMECE2002-33625

ANALYTICAL SOLUTION OF THE FLOW ALONG PARALLEL MICROCHANNELS SEPARATED BY A POROUS MEMBRANE

Changgu Lee and Luc G. Fréchette
Columbia University
Department of Mechanical Engineering
500 West 120th Street, New York NY, 10027

ABSTRACT

This papers presents the analytical solution of the flow distribution along a porous membrane which is between two parallel microchannels, a configuration of increasing importance in microsystems for DNA sequencing, catalytic chemistry, and in micro heat exchangers. The modeling approach presented in the paper is inspired from thin film lubrication theory and would be applicable for a wide range of low Reynolds number, pressure-driven microfluidic configurations.

Keywords: Microfluidics, MEMS, microchannel, porous membrane, low Reynolds number.

INTRODUCTION

Microfabrication and MEMS technology are expanding their application beyond sensors and actuators enabling a broad range of integrated microsystems. Some may include complex microfluidic circuits, composed of various components such as straight channels, expansions and contractions, multiple to single channel distributors and collectors, valves, fluidized packed beds, mixers, heaters, and through flow membranes. Although fluid flow in straight microchannels has received significant interest, other components are less well characterized. In this paper, the pressure and through flow distributions over a thin, planar membrane are studied analytically, providing design guidelines for basis for low Reynolds number, pressure driven fluidic microsystems.

Membranes can be used in a wide range of applications that either require high surface area relative to other fluidic components or large planar distribution. Applications are found in the following areas: (1) biological and biomedical: DNA sequencing, low particle count sensing; (2) chemical: well-controlled chemical processing using surface catalysts, micro fuel cells; (3) thermal: high heat flux micro heat exchangers and micro jet arrays for cooling.

At traditional scales, membranes typically consist of thin sheets of isotropic porosity held between with large supply and collection plena. The flow velocities in the plena are typically negligible and the pressures uniform. The flow rate is therefore uniform over the membrane area, since it is directly proportional to the pressure difference across it. In microfabricated systems, the thickness of the plena is limited by maximum practical etch depths and the substrate thickness. Also, the planar nature of microfabrication constrains the inlet and outlet ports to be located in the corners or edges of the membrane area. These limitations can result in pressure non-uniformity over the membrane area due to viscous pressure drop in the plena, which in this case, are best referred to as channels. Non-uniform pressure distribution will result in non-uniform flow across the membrane area.

Development of increasingly complex microfluidic circuits will require efficient and accurate representation of the various components. Numerical tools (CFD) specifically developed for low Reynolds number (Stokes) flow are available and will be useful in analyzing complex microfluidic systems. Generally, low order modeling is preferable to discretized computational modeling, since it allows rapid design of microfluidic circuits with the high level of complexity enabled by microfabrication. Detailed numerical analysis tools (CFD) would complement low order design tools to verify or validate the final design or model components less tractable analytically.

Although solutions are commonly available for straight microchannels [1-3] other components in microfluidic circuits have not received the same level of attention [4,5]. Here, the analytical solution for the flow field along the supply channel, through a thin membrane, and along the collection channel is presented, and validated with validated by comparison with the numerical solution (CFD). First, the analytical development is presented, identifying the main non-dimensional parameter. Then, results in a non-dimensional form are presented and discussed, and general design guidelines are outlined. Although the specific analysis is developed for the membrane configuration, the approach forms a basis for the analysis of other configurations or components in microfluidic circuits.

NOMENCLATURE

A = th^3/aL^2 non-dimensional resistance parameter
L = length of membrane
P = Pressure
$\overline{P}$ = non-dimensional pressure
$\vec{U}$ = velocity vector
V = velocity through membrane
$\overline{V}$ = non-dimensional velocity through membrane
h = channel height
t = thickness of membrane
u = velocity component in x-direction
v = velocity component in y-direction

Greek symbols

a = permeability (m^2)
m = viscosity ($N \cdot s/m^2$)
r = density

Subscripts

1: upper channel (supply)
2: lower channel (collector)
in: inlet of upper channel (x=0)
out: outlet of lower channel (x=L)

PROBLEM FORMULATION

The focus is on solving for the velocity and pressure profiles of two-dimensional, steady, incompressible, low Reynolds number flow along two parallel microchannels, which share a common porous thin wall or membrane (Fig. 1). As the fluid travels along one channel (upper), it gradually passes through the porous membrane and is collected along the second channel (lower). The local normal velocity through the membrane is driven by the local pressure difference, $\Delta P(x)=P_1(x)-P_2(x)$, between the upper and lower channels at a specific axial location, x. The type of membrane considered here consists of an anisotropic thin region that allows a through flow velocity, $V(x)$, proportional to the pressure difference (Darcy's law), but no flow along the length of the membrane nor slip tangential to its surfaces. Practically, these assumptions represent a porous membrane formed as an array of holes or pores normal to the membrane surface.

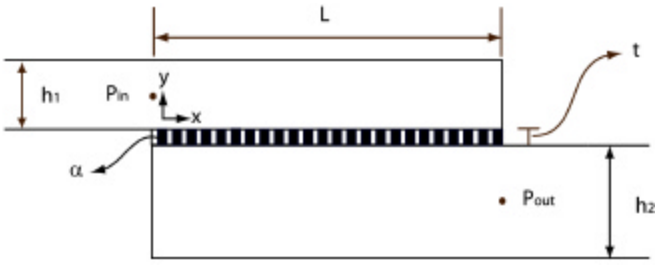

Figure 1 - Schematic cross-section of the throughflow membrane configuration studied here. Flow is from left to right: entering the upper channel, gradually flowing through the membrane, and along the lower channel (thickness is exaggerated for illustration purposes).

ANALYTICAL DEVELOPMENT

The pressure distribution along each channel is determined from the mass and momentum conservation equations, by applying the classic approach used by O. Reynolds [6] in hydrodynamic lubrication theory [1], which neglects inertial forces and assumes average flow values across the film thickness. This last aspects is probably the most important. The differential equations of motion and mass conservation are integrated across the film thickness, effectively reducing the dimensionality of the problem. This approach was also central to the boundary layer integral momentum theory, proposed by von Karman.

Researchers in the field of tribology have extensively analyzed thin fluid films based on the Reynolds equation, or modified versions that consider porous walls [7,8]. These analyses considered the wall as a thick porous medium with isotropic porosity [9-11], with a uniform back pressure. The analytical development presented here is essentially based on a modified Reynolds equation, although formulated to account for non-uniform pressure in both channels and for a membrane that only allows normal throughflow, hence anisotropic porosity.

In this section, the equations of motion are first simplified for microchannel flow, assuming the pressure to be uniform across the channel and the normal velocity gradient to dominate. Based on these simplifications, the velocity profiles are determined through integration. These are then substituted in integrated form of the mass conservation equation. Applying this approach along both channels, imposing mass conservation across the membrane, and introducing the appropriate pressure boundary conditions leads to a linear system of eight equation, which are then solved for.

First, the incompressible form of the Navier-Stokes equations:

$$r\frac{D\vec{U}}{Dt} = -\nabla P + m\nabla^2\vec{U} \qquad (1a)$$

and continuity equation:

$$\nabla \cdot \vec{U} = 0 \qquad (1b)$$

are simplified according to the following assumptions:

1) low Reynolds number flow, such that the non-linear convective acceleration terms can be neglected;
2) steady-state flow;
3) incompressible flow and uniform fluid properties;
4) two-dimensional geometry and flow field, Fig. 1 is therefore the cross-section of a rectangular membrane with inlet and outlet ports along opposite edges, and sufficiently wide for end effects to be negligible.
5) channel length is much greater than its height, $h/L << 1$, such that velocity gradients in the y-direction dominate: $d/dx << d/dy$;
6) pressure is uniform across the height of each channel, hence only varies in the x-direction: $P_1(x)$, $P_2(x)$
7) flow through the membrane obeys Darcy's law in the y-direction, but does not allow flow nor slip in the x-direction.

The simplified Navier-Stokes equations for channel flow are then:

$$\text{X-dir: } \frac{dP}{dx} = \frac{\partial}{\partial y}(m\frac{\partial u}{\partial y}) \tag{2a}$$

$$\text{Y-dir: } 0 = m\frac{\partial^2 v}{\partial y^2} \tag{2b}$$

and the continuity equation becomes:

$$\frac{\partial u}{\partial x} + \frac{\partial v}{\partial y} = 0 \tag{2c}$$

The following analysis is applied for both channels, shown first for the upper one. The x-direction velocity profile, *u(x,y)*, is determined by integrating Eqn (2a) with the no-slip condition, $u=0$, at $y=0$ and $y=h_1$, yielding a parabolic profile:

$$u = \frac{1}{2m}\frac{dP_1}{dx}y(y-h_1) \tag{3}$$

The y-direction velocity profile, *v(x,y)*, can also be determined by integrating Eq. (2b) with $v=V(x)$ at $y=0$ (membrane throughflow velocity) and $v=0$ at $y=h_1$, resulting in a linear velocity profile normal to the membrane:

$$v = -V(x)(\frac{y}{h_1} - 1) \tag{4}$$

The continuity Eq. (2c) is then integrated across the channel height (y-direction) from *0* to h_1 and the expressions derived for *u* and *v* are substituted, resulting in;

$$\int_0^{h_1}(\frac{\partial u}{\partial x} + \frac{\partial v}{\partial y})dy = -\frac{{h_1}^3}{12m}\frac{d^2P_1}{dx^2} - V(x) = 0 \tag{5}$$

The membrane throughflow velocity can then be expressed as a function of the pressure is the upper and lower channels: $P_1(x)$ and $P_2(x)$ respectively. Darcy's law is applied to represent the membrane, stating that the velocity is directly proportional to the pressure gradient, according to the fluid viscosity, *m*, and membrane permeability, *a*:

$$\nabla P = -\frac{m}{a}V(x)$$

$$\frac{\Delta P}{t} = -\frac{m}{a}V(x)$$

$$-V(x) = \frac{a}{t\times m}\Delta P = \frac{a}{t\times m}(P_1 - P_2) \tag{6}$$

Therefore, Eq. (5) becomes

$$\frac{{h_1}^3}{12m}\frac{d^2P_1}{dx^2} = \frac{a}{t\times m}\left(P_1(x) - P_2(x)\right) \tag{7}$$

Equation (7) is the pressure equation for the upper, or supply, channel. By the same process, the resulting pressure equation for the lower, or collector, channel is:

$$\frac{{h_2}^3}{12m}\frac{d^2P_2}{dx^2} = -\frac{a}{t\times m}\left(P_1(x) - P_2(x)\right) \tag{8}$$

If the coefficients of the right side terms of Eqs. (7) and (8) are moved to the left hand side, and the two equations are non-dimensionalized, they become:

$$\frac{t\times {h_1}^3}{12aL^2}\frac{d^2\overline{P}_1}{d\overline{x}^2} = \overline{P}_1 - \overline{P}_2 \tag{9}$$

$$\frac{t\times {h_2}^3}{12aL^2}\frac{d^2\overline{P}_2}{d\overline{x}^2} = -(\overline{P}_1 - \overline{P}_2) \tag{10}$$

where the non-dimensional variables are $\overline{x} = x/L$, $\overline{P}_i = (P_i - P_{out})/(P_{in} - P_{out})$. The coefficient before the second derivative of pressure defines a non-dimensionalized parameter, as:

$$A_i = \frac{t\times {h_i}^3}{12aL^2} \quad (\text{for } i=1,2) \tag{11}$$

Equations (9) and (10) have two pressure variables, one of which can be removed by combining the equations into one, resulting in a fourth order differential equation in $P_1(x)$:

$$A_1A_2\overline{P}_1^{(4)} - (A_1 + A_2)\overline{P}_1^{(2)} = 0 \tag{12}$$

The general solution of Eq. (12) is of the form:

$$\overline{P}_1 = a_1 + b_1\overline{x} + c_1e^{\overline{x}\sqrt{\frac{A_1+A_2}{A_1A_2}}} + d_1e^{-\overline{x}\sqrt{\frac{A_1+A_2}{A_1A_2}}} \tag{13}$$

where $\sqrt{\frac{A_1+A_2}{A_1A_2}}$ can be expressed as $\sqrt{\frac{1}{A_1}(1+\frac{{h_1}^3}{{h_2}^3})}$, such that Eq. (13) is written as:

$$\overline{P}_1 = a_1 + b_1\overline{x} + c_1e^{\overline{x}\sqrt{\frac{1}{A_1}(1+\frac{{h_1}^3}{{h_2}^3})}} + d_1e^{-\overline{x}\sqrt{\frac{1}{A_1}(1+\frac{{h_1}^3}{{h_2}^3})}} \tag{14}$$

The same process expresses the solution for pressure in the lower channel as follows:

$$\overline{P}_2 = a_2 + b_2\overline{x} + c_2e^{\overline{x}\sqrt{\frac{1}{A_1}(1+\frac{{h_1}^3}{{h_2}^3})}} + d_2e^{-\overline{x}\sqrt{\frac{1}{A_1}(1+\frac{{h_1}^3}{{h_2}^3})}} \tag{15}$$

Pressure Boundary Conditions

To define the coefficients of the pressure Eqs. (14) and (15), four (4) boundary or matching equations are needed for each channel. The four relations are as follows;

1) Inlet and outlet pressure

$$\begin{aligned}\overline{P}_1(\overline{x}=0) &= 1\\ \overline{P}_2(\overline{x}=1) &= 0\end{aligned} \tag{16}$$

2) Wall boundary conditions - At the closed end of each channel, $U_1(x=1) = U_2(x=0) = 0$, therefore from Eqn (3):

$$\begin{aligned}\frac{d\overline{P}_1}{d\overline{x}}(\overline{x}=1) &= 0\\ \frac{d\overline{P}_2}{d\overline{x}}(\overline{x}=0) &= 0\end{aligned} \tag{17}$$

3) Mass Conservation - The flow rates at inlet, outlet, and through the membrane should be the same:

$$\begin{aligned}\int_0^{h_1}u_1dy &= \int_0^L Vdx\\ \int_{h_2}^0 u_2dy &= \int_0^L Vdx\end{aligned} \tag{18}$$

4) Equations (9) and (10) must be met at the inlet and exit axial locations:

$$\left.\frac{d^2\overline{P}_1}{dx^2}\right|_{\overline{x}=0} = \frac{1}{A_1}\left(\overline{P}_{in} - \overline{P}_2(\overline{x}=0)\right) \tag{19a}$$

$$\left.\frac{d^2\overline{P}_2}{dx^2}\right|_{\bar{x}=1} = -\frac{1}{A_2}\left(\overline{P}_1(\bar{x}=1) - \overline{P}_{out}\right) \qquad (19b)$$

The above boundary and matching conditions, Eqs (16) to (19) are applied to each pressure equation, resulting in eight linear equations, function of eight coefficients: {a_1, b_1, c_1, d_1, a_2, b_2, c_2, d_2}. Solving for a closed analytical form of these coefficients by recursive substitution is tractable, but the complex expressions are not found to provide much insight, other than showing that the coefficients are a function of {A_1, h_1/h_2}. They are instead solved in numerical form for specified values of {A_1, h_1/h_2}, by casting the set of equations in matrix form: $[D]\cdot\vec{c} = \vec{b}$, with $\vec{c}$ as a vector of the eight coefficients and $\vec{b}$ the vector of right hand sides, and multiplying each side by the inverse matrix D^{-1}.

RESULTS AND DISCUSSION

As formulated, the solution will solely be a function of the non-dimensional groupings {A_1, A_2}. Since these two non-dimensional numbers are simply related by the ratio of channel heights, h_1/h_2, an alternate set of main parameters can be {A_1, h_1/h_2}. Results are therefore presented next for ranging values of {A_1, h_1/h_2}. Parameter A_1, which results from the analytical development, represents the *ratio of membrane throughflow resistance to channel flow resistance*. Flow behavior is therefore expected to vary when this parameter ranges from greater than to less than unity. The coefficients that appear in the exponentials of Eqs (13), (14) or (15) represent the ratio of total resistance for both channels to the membrane flow resistance:

$$\frac{A_1 + A_2}{A_1 A_2} = \frac{1}{A_1} + \frac{1}{A_2} = \frac{R_{upper,channel} + R_{lower,channel}}{R_{membrane}} \qquad (20)$$

In the following study, A_1 is used instead of this more global non-dimensional parameter since it better decouples the ratio of channel heights.

Effect of non-dimensional parameter - *A*

Figure 2 shows the resulting static pressure profile along both channels (-) and the through flow velocity distribution (--) along the membrane for a range of A_1 values and symmetric channel heights (h_1/h_2=1). Figure 2 (b) identifies the curves depicted. The results presented are generic for any set of geometric and operating parameters that yield the same A_1 through the choice of non-dimensional axes. The pressure difference across the membrane, Ä*P(x)* = *P*$_1$*(x)*-*P*$_2$*(x)*, scales linearly with the throughflow velocity, *V(x)*. The non-uniform pressure profiles therefore result in higher through flow

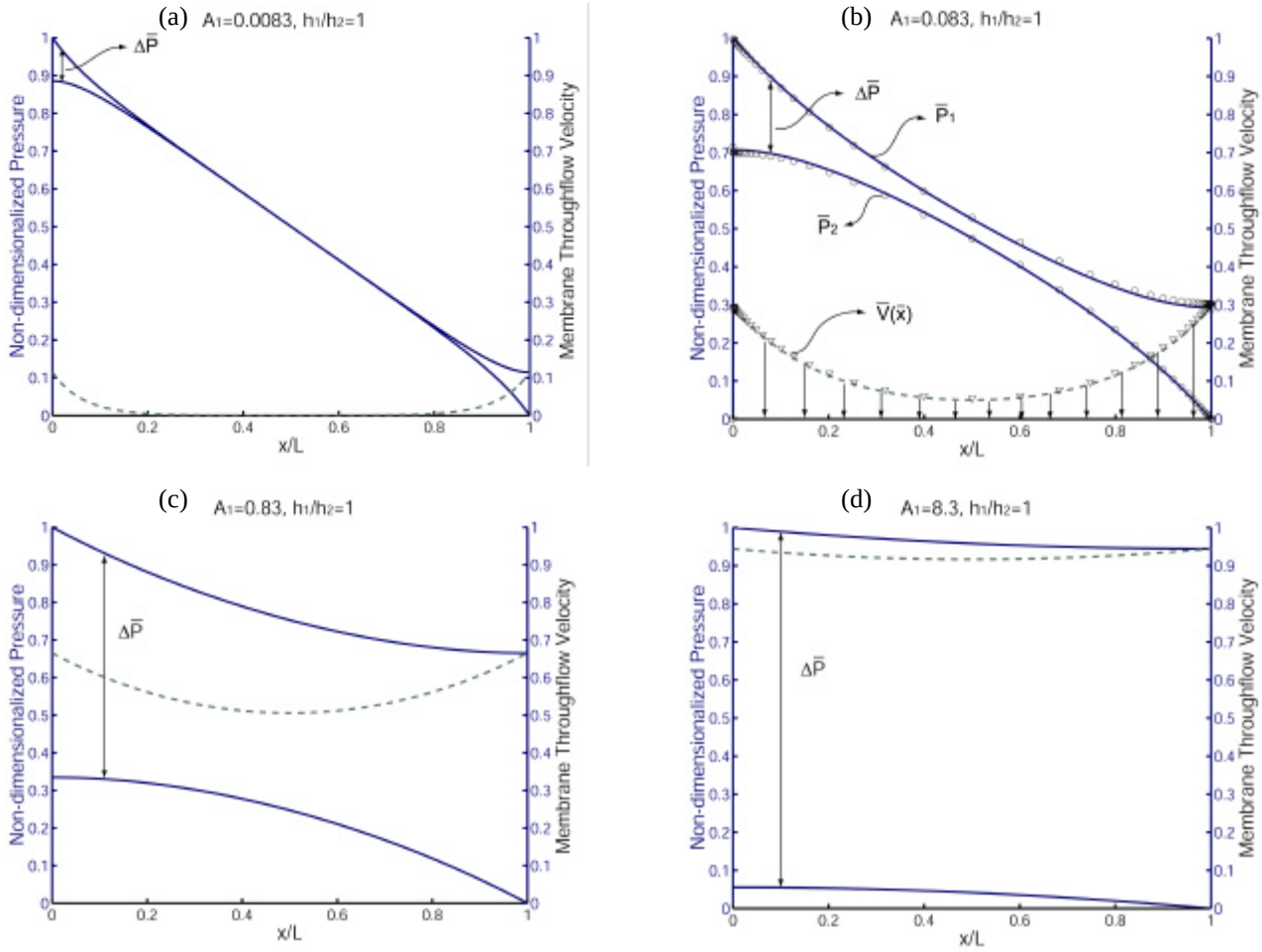

Figure 1 - Profiles of pressure along the upper and lower channels (-) and membrane throughflow velocity distribution (--) for varying values of A_1={0.0083, 0.083, .83, 8.3} and equal channel heights (h_1=h_2).

velocities, whereas for most applications, a uniform through flow velocity would be desirable.

At low values of A_1, Fig. 2 (a), the channel flow resistance dominates and the flow preferentially traverses near the ends of the channel. Given the symmetry, the flow is split between the beginning and end of the membrane area. In the center region, flow preferentially travels along the channel, as characterized by the constant pressure gradient typical of fully developed, incompressible channel flow with constant flow rate. In contrast for large values of A_1, Fig. 2 (d), pressures in the channels tend to be uniform, leading to a uniform pressure difference and throughflow over the membrane area. $V(x)$ varies by less than 5% over the entire length, for the value shown (A_1 = 8.3). Physically, this case corresponds to increasing channel height (large plena) or lower membrane resistance (t/a). One should note that fluid viscosity does not come into play, since both the channel and membrane resistances are proportional to it.

At intermediate values of A_1 =0.083 and 0.83 in Fig. 2 (b) and (c) respectively, the solution shows a combination of both extremes, with a noticeable pressure drop along the channels and moderate throughflow velocity non-uniformity. Flow uniformity improves with larger A_1 values.

Effect of Channel Height Ratio - h_1/h_2

Similar upper and lower channel heights are sometimes impractical due to microfabrication constraints. This section therefore evaluates the impact of the channel height ratio, h_1/h_2, on the membrane throughflow distribution. Results are shown in Fig. 3, for a nominal value of A_1 = 0.083 (kept constant) and h_1/h_2 varying in the range {1/4… 4}.

In the of case of shallower upper channels (h_1/h_2 < 1) in Fig. 3 (a) and (b), most of the flow crosses the membrane near the inlet (x=0) since the upper channel acts as a relatively high resistance. Another view is that the pressure drop along the upper channel is more than that along the deeper, bottom channel, resulting in a larger pressure difference near the inlet. This induces a significant increase in flow non-uniformity,

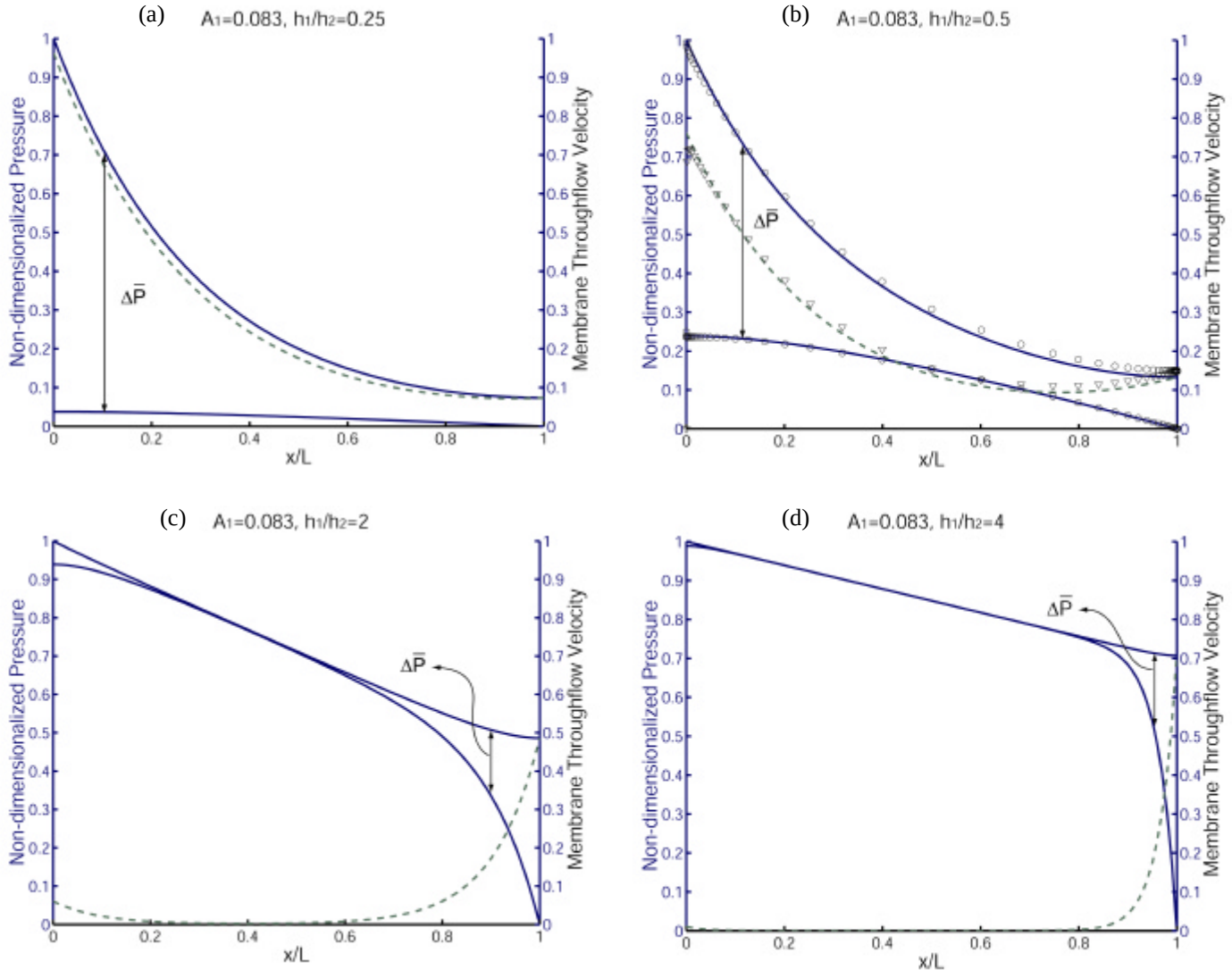

Figure 3 - Profiles of pressure along the upper and lower channels (-) and membrane throughflow velocity distribution (--) for varying values of channel height ratio h_1/h_2={0.25, 0.5, 2, 4} and constant A_1= 0.083.

compared to the case with symmetric channel heights, Fig 2(b).

For deeper upper channels ($h_1/h_2 > 1$) shown in Fig. 3 (c) and (d), flow preferentially travels along the upper channel to cross the membrane near the outlet ($x=L$). Similarly to the other case, this induces undesirable throughflow non-uniformity. A noticeable difference however is the practically inexistant flow in the first 3/4 of the membrane area. For similar, but reversed channel heights in Fig. 3 (a) and (b), non-negligible flow was present over the entire extent of the membrane area. Given the choice between a relative channel height less or more than unity, shallower supply channel seems preferable ("upper" refers to the supply channel).

Flow Field

A typical flow field is illustrated in Fig. 4 for: $A_1 = 0.083$ and $h_1/h_2 = 1$ (case shown in Fig. 2 (b)). Velocity vectors are plotted at different axial locations along both channel, as well as the resulting streamlines. Velocities are determined from Eqs (3) and (4), once the pressure gradient and membrane throughflow velocity have been solved for. The velocity field is therefore the combination of a parabolic x-direction velocity profile with a linear y-direction velocity profile. At lower A_1 = values, more flow would be diverted towards the channel ends, with axial flow in the center region.

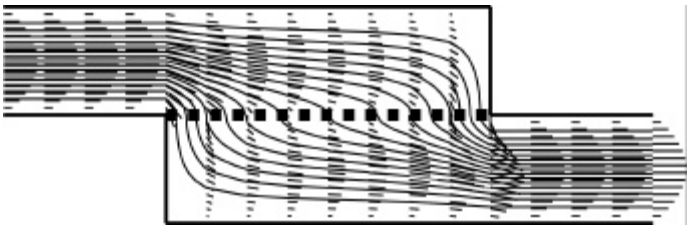

Figure 4 – Streamlines and velocity vectors in a nominal case. Flow enters from the left, travels along the upper channel, through the membrane, and out the lower channel (thickness has been exaggerated for clarity, L/h is actually 100).

Comparison to Numerical Solution

In order to validate this analytical approach, these results were compared to numerical solutions of the Navier-Stokes equations in an identical configuration, using a commercial code [12]. The computational domain consisted of three zones: the upper channel, lower channel, and a zone of thickness t between them as the membrane. The boundary conditions simply consisted of inlet and outlet pressures. The membrane zone was modeled as an isotropic porous media of permeability a, and with a negative source term added to the x-momentum equation in order to prevent any flow along the membrane extent. Therefore, the flow in the membrane zone becomes purely in the y-direction.

Numerical results are overlaid in Figures 2 (b) and 3 (b) as the circles and crosses, showing very good agreement with the analytical modeling predictions. As long as the main assumptions listed earlier are satisfied, the analytical approach is therefore shown to be valid.

CONCLUSIONS

A relatively straightforward approach was developed to analytically predict the pressure distributions along two parallel microchannels separated by a porous membrane, typical of applications such as DNA sequencing [13]. The resulting throughflow velocity distribution over the membrane extent was studied as a function of the operating regime and relative heights of the supply and collection channels. A central non-dimensional parameter is the ratio of membrane flow resistance to channel flow resistance. Low values of this parameter, as well as different channel heights are shown to increase the membrane throughflow non-uniformity, and more so when the supply channel is deeper than the collector channel. Analytical results were successfully compared to computational fluid dynamics solutions to validate the development.

This analysis could also be extended to address non-uniform channel geometry, allowing one to tailor the throughflow velocity profile by changing the channel height or width in order to satisfy application requirements. This analytical approach, based on integral momentum or lubrication theory, appears to be relatively versatile and amendable for a broader range of microfluidic geometries.

REFERENCES

[1] Constantinescu, V.N., 1995, *Laminar Viscous Flow*, Springer-Verlag, New York.

[2] Ho, C.M., and Tai, Y.C., 1998, *Ann. Rev. Fluid Mech.*, **30**, pp. 579-612.

[3] Pfahler, J., Harley, J., Bau, H.H., Zemel, J., 1990, "Liquid Transport in Micro and Submicron Channels", *Sensors and Actuators*, **A21-A23**, 431.

[4] Li, X., Lee, W.Y., Wong, Man, Zohar, Y., 2001, "Pressure losses in microchannels with bends", *Proc. 14th Int'l Conf. on Micro Electro Mechanical Systems*, Interlaken, Switzerland, pp. 491-494.

[5] Li, X., Lee, W.Y., Wong, Man, Zohar, Y., 2001, "Flow separation in constriction microchannels", *Proc. 14th Int'l Conf. on Micro Electro Mechanical Systems*, Interlaken, Switzerland, pp. 495-498.

[6] Reynolds, O., 1886, "On the theory of lubrication and it's application to Mr. Beauchamp Tower's experiments", *Philos. Trans. R. Soc. London*, **177**, part I, pp. 157-234.

[7] Cameron, A., Morgan, V. T., and Stainsby, A. E., Critical Conditions for Hydrodynamic Lubrication of Porous metal Bearings, Institution of mechanical Engineers-Proceedings, **176**, Nov. 28, 1962, pp. 761-770.

[8] Morgan, V. T., and Cameron, A., Mechanism of Lubrication in Porous Metal Bearings, 1957 Conference on Lubrication and Wear, Institution of Mechanical Engineers, London, U. K., Paper 89, pp. 151-157.

[9] J. Prakash and S. K. Vij, Squeeze Films in Porous Bearings, Wear, 27, 1974, pp 357-366.

[10] C. Cusano, Lubrication of Porous Journal Bearings, Journal of Lubrication Technology, 1972, pp 69-73.

[11] Rouleau, W. T., Hydrodynamic Lubrication of Narrow Press-Fitted porous Metal Bearings, Journal of Basic Engineering, Trans. ASME, Series D, **85**, No. 1, mar. 1963, pp. 123-128.

[12] Fluent v.5 software by Fluent, Inc., Lebanon, NH.

[13] Brady J. Cheek, Adam B. Steel, Matthew P. Torres, Yong-Yi Yu, and Hongjun Yang, Chemiluminescence Detection for Hybridization Assays on the Flow-Thru Chip, a Three-Dimensional Microchannel Biochip, Anal. Chem. 2001, **73**, pp 5777-5783.